PAPER

Effects of manganese doping on the structure evolution of small-sized boron clusters

View the article online for updates and enhancements.

Effects of manganese doping on the structure evolution of small-sized boron clusters

Lingquan Zhao[1,2,7]**, Xin Qu**[4,5,7]**, Yanchao Wang**[3]**, Jian Lv**[1,8]**, Lijun Zhang**[1]**, Ziyu Hu**[6,8]**, Guangrui Gu**[2,8] **and Yanming Ma**[3]

[1] College of Materials Science and Engineering, Jilin University, Changchun 130012, People's Republic of China
[2] Department of Physics, College of Science, Yanbian University, Yanji 133002, People's Republic of China
[3] State Key Laboratory of Superhard Materials, Jilin University, Changchun 130012, People's Republic of China
[4] Changchun Institute of Optics, Fine Mechanics and Physics, Chinese Academy of Sciences, Changchun 130033, People's Republic of China
[5] University of Chinese Academy of Sciences, Beijing 100039, People's Republic of China
[6] Beijing Computational Science Research Center, Beijing 100084, People's Republic of China

E-mail: lvjian@jlu.edu.cn, grgu@ybu.edu.cn and huziyu@csrc.ac.cn

Abstract

Atomic doping of clusters is known as an effective approach to stabilize or modify the structures and properties of resulting doped clusters. We herein report the effect of manganese (Mn) doping on the structure evolution of small-sized boron (B) clusters. The global minimum structures of both neutral and charged Mn doped B cluster MnB_n^Q ($n = 10$–20 and $Q = 0, \pm1$) have been proposed through extensive first-principles swarm-intelligence based structure searches. It is found that Mn doping has significantly modified the grow behaviors of B clusters, leading to two novel structural transitions from planar to tubular and then to cage-like B structures in both neutral and charged species. Half-sandwich-type structures are most favorable for small $MnB_n^{-/0/+}$ ($n \leqslant 13$) clusters and gradually transform to Mn-centered double-ring tubular structures at $MnB_{16}^{-/0/+}$ clusters with superior thermodynamic stabilities compared with their neighbors. Most strikingly, endohedral cages become the ground-state structures for larger $MnB_n^{-/0/+}$ ($n \geqslant 19$) clusters, among which MnB_{20}^+ adopts a highly symmetric structure with superior thermodynamic stability and a large HOMO-LUMO gap of 4.53 eV. The unique stability of the endohedral MnB_{20}^+ cage is attributed to the geometric fit and formation of 18-electron closed-shell configuration. The results significantly advance our understanding about the structure and bonding of B-based clusters and strongly suggest transition-metal doping as a viable route to synthesize intriguing B-based nanomaterials.

Keywords: *ab initio* calculations, manganese-doped boron clusters, endohedral cages

S Supplementary material for this article is available online

(Some figures may appear in colour only in the online journal)

---

[7] Equally share the first authorship
[8] Author to whom any correspondence should be addressed.

1. Introduction

Boron is an element of intriguing structural and chemical complexity that never ceases to surprise us. Because of its electron deficiency nature, a rich variety of structures at different dimensions along with unusual bonding situations can be formed. Besides the sixteen polymorphs of boron that have been reported at ambient condition [1], low-dimensional systems, such as 2D sheet [2] and 1D nanotubes [3–6] have been fabricated. For 0D clusters, combined experimental and theoretical studies during the last few decades have established that small-sized boron clusters are planar or quasi-planar [7–17], whose stabilities can be rationalized in terms of aromaticity and antiaromaticity similar to those of polycyclic hydrocarbons [18, 19]. This is in contrast to the bulk boron solids and boron-rich compounds, where 3D cage-based structures are prevalent [1, 20]. Transitions from planar to double-ring tubular structures have been reported at B_{16} for cation [21] and B_{20} for neutral species [22]. But anionic born clusters (e.g. B_{27}^-, B_{30}^-, B_{35}^- and B_{36}^-) still possess quasi-planar structures [23–26]. More strikingly, boron fullerene analogues (borospherene) have been theoretically proposed at B_{38} [27] and experimentally observed at B_{40} [28]. A series of axially chiral borospherenes, B_{39}^-, B_{41}^+ and B_{42}^{2+}, were subsequently identified [29, 30], and the smallest borospherene was even observed at B_{28} [15].

Atomic doping of clusters is known as an effective approach to stabilize or modify the structures and properties of resulting doped clusters. Given the rich structural diversity of boron clusters, a series of metal doped boron clusters with intriguing structure and bonding patterns have been discovered along this line. Due to the closed-shell electronic structure and aromaticity of planar B_3^-, B_8^{2-}, B_9^-, B_{10}, B_{11}^- and B_{12} clusters, they were suggested to be promising candidates for new inorganic ligands or building blocks [31], and series of half-sandwich and sandwich-type complexes have been designed via metal doping of these planar species. Half-sandwich-type structures have already been experimentally confirmed to be the ground states for CoB_{12}^- and RhB_{12}^-, where the B_{12} ligands have the similar structure as the bare B_{12} clusters [32]. The wheel-type geometries of B_8^{2-} and B_9^- cluster [16] lead to the discovery of a series of transition-metal-centered borometallic molecular wheels: FeB_8^- [33], FeB_9^- [33], CoB_8^- [34], RuB_9^- [34], RhB_9 [35], IrB_9 [35], NbB_{10}^- and TaB_{10}^- [36], where the NbB_{10}^- and TaB_{10}^- hold the highest coordination number in planar molecular species. Moreover, double-ring tubular structures are also realized in Co and Mn doped B_{16} anionic clusters, which have the highest coordination number (16) known heretofore in chemistry [37, 38]. Recently, simulated by the discovery of borospherene, extensive metal doping for B_{38} and B_{40} clusters have been carried out theoretically, suggesting the formation of a series of endohedral and exohedral boronfullerenes [39–43], and even the possibilities of stabilization of small boron fullerenes (e.g. FeB_{20} [44], MoB_{24} and WB_{24} [45] clusters) have been proposed.

It is seen that metal doping has significantly enriched the structures of boron clusters. Some peculiar geometries can be formed when appropriate metal atom is incorporated. Considering the fact that different metal atoms have different effect on modifying the structures of B clusters through both geometric and electronic factors, it is reasonable to expect that the profile of potential energy landscape of B clusters will be changed significantly when different metal atom is incorporated. In the current work, we systematically investigated the structure evolution of neutral and charged Mn doped boron clusters, MnB_n^Q with $n = 10$–20 and $Q = 0$, ± 1, through extensively swarm-intelligent global structure searches combined with first-principles density functional calculations. Two structural transitions of B structure from planar to tubular and then to cage-like structures have been revealed for both neutral and charged species in this size range. Binding energy calculations indicate that $MnB_{16}^{+/0/-}$ clusters with Mn-centered double-ring tubular structures are energetically more stable than its neighbors regardless of the charge states, indicating the robustness of the tubular geometry when Mn is doped. Intriguingly, highly symmetric endohedral B cage with superior thermodynamic stability and closed-shell electronic configuration has been found to be the global minimum structure for the MnB_{20}^+ cluster.

2. Computational details

Our approach involves global minimization of the potential energy surfaces, merging *ab initio* total energy calculations via CALYPSO cluster prediction [46–48] based on the particle swarm optimization algorithm implemented in the CALYPSO code. Several techniques are included in the algorithm to improve the search efficiency, e.g. point group symmetry constraints in structural generation, bond characterization matrix technique for fingerprinting structures, and local version of the particle swarm optimization algorithm enabling simultaneous search in different energy funnels, etc [48]. Its validity has been manifested by its successfully identifying the ground-state structures for a series of cluster systems [27, 45]. The underlying energy calculations and structure relaxations were performed in the framework of density functional theory (DFT) using the Gaussian 09 Package [49]. During the structure searches, hybrid PBE0 [50] functional was used. Singlet and doublet spin states were selected for cluster with even and odd number of electrons, respectively, along with Stuttgart basis set for Mn and 3–21 basis set for B. Then, refined structural optimizations and vibrational frequency calculations at different spin states for low-lying isomers were performed at $PBE0/Mn/Stuttgart/B/6–311 + G^*$ level of theory. At this step, singlet, triplet and quintet states were considered for clusters with even number of electrons, while doublet, quartet and sextet states were considered for clusters with odd number of electrons. It is found that refined structural optimizations sometimes modified the energetic order of the predicted structures within ~0.05 eV/atom. To confirm the lowest-energy structure, predicted low-lying isomers within ~2 eV of the global minimum have been subject to refined structural optimizations. In a previous benchmark calculation,
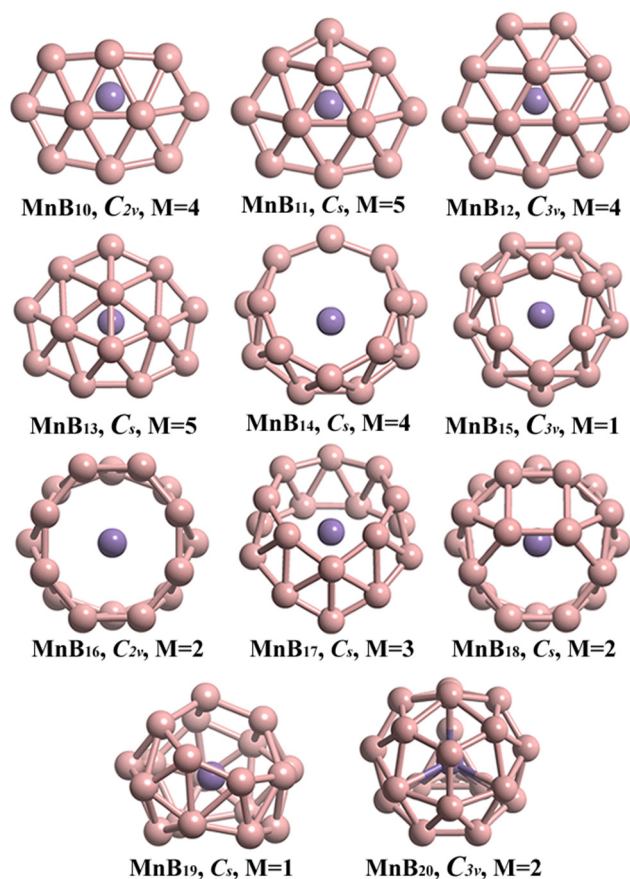
Figure 1. Lowest-energy structures of MnB$_n$ ($n = 10$–20) clusters from the structure searches. For each structure, the point group symmetry and spin multiplicity (M) are indicated.

the PBE0 was confirmed to be suitable for describing the energy difference of isomers of medium-sized boron clusters (e.g. B$_{20}$) compared to the high-level CCSD(T) results [51].

3. Results and discussion

3.1. Geometrical structures

The global minimum structures for MnB$_n^Q$ ($n = 10$–20 and $Q = 0, \pm1$) clusters from current structure searches are shown in figures 1–3, along with their point group symmetries and spin multiplicity values. Other low-lying isomers are given in figures S1–S3 in the supplementary data (stacks.iop.org/JPhysCM/29/265401/mmedia). Generally speaking, Mn doping has fundamentally modified the grow behaviors of B clusters. The B structures in both neutral and charged MnB$_n$ ($n = 10$–20) clusters exhibit two structural transitions from planar to tubular and then to cage-like structures. This is in stark contrast to the pure B clusters in the same size range, where all anionic species possess planar structures [18], and cationic species only exhibit a planar to tubular structural transition at B$_{16}$ [21]. The ground states of MnB$_n^{+/0/-}$ clusters with $n < 15$ generally exhibit high spin states, e.g. quintets for cluster with even number of electrons and quartets for clusters with odd number of electrons, while larger MnB$_n^{+/0/-}$

($n > 15$) cluster prefer lower spin states (singlets or triplets for even number of electrons and doublets for odd number of electrons).

For neutral MnB$_n$ clusters, half-sandwich-type structures emerge at $n = 10$–13 with the quasi-planar B$_n$ moieties coordinating to the Mn atom (figure 1). The B atoms in MnB$_{10}$ cluster exhibit a similar quasi-planar structure as that of bare B$_{10}$ cluster with two B atoms located in an 8-memberd ring [17]. The MnB$_{11}$ and MnB$_{12}$ clusters can be seen as adding one and two B atoms on the lateral of the B$_{10}$ moiety in MnB$_{10}$ cluster, and both of them possess three inner B atoms. While the structure of B$_{11}$ moiety in MnB$_{11}$ is different from that of bare B$_{11}$ cluster, the structure of B$_{12}$ moiety in MnB$_{12}$ is exactly same as that of bare B$_{12}$ cluster with high point group symmetry of C$_{3v}$ [17]. This is in accordance with the experimental observation that the aromatic B$_{12}$ cluster with electronic structure analogues to benzene are highly chemically stable and can be used as inorganic ligand to form half-sandwich-type structures with transition metals [17, 32]. Inserting additional inner B atom into the B$_{12}$ moiety of MnB$_{12}$ cluster leads to the formation of MnB$_{13}$ with four inner B atoms. The B structures in MnB$_{14}$ and MnB$_{15}$ are much different from those of smaller MnB$_n$ clusters. They exhibit bowl-like B structures but with 8-membered and 6-memebered B rings, respectively, which can be seen as intermediate structures between quasi-planar and tubular structures. The well-known double-ring tubular structure with the Mn atom located at the center of the tube occurs at MnB$_{16}$, having a point group symmetry of C$_{2v}$, which is in agreement with previous joint experimental and theoretical study [37]. Earlier theoretical study has found that iron (Fe) doping of B clusters even produced double-ring tubular structure at smaller size of $n = 14$ [44]. Since the atomic radius of Fe (1.32 Å) is slight smaller than that of Mn (1.39 Å), in view of geometric point it is expected that the formation of perfect double-ring tubular structure is closely related to the size of the doping atom. MnB$_{17}$ cluster still possesses a tubular structure with an additional B atom inserted into the double-ring B tube of MnB$_{16}$ cluster, and MnB$_{18}$ can be seen as MnB$_{16}$ with two additional capped B atoms. As the number of B atoms increasing, B cages with Mn atom encapsulated are formed at $n = 19$ and 20.

As depicted in figures 2 and 3, the grow behaviors of cationic and anionic MnB$_n$ clusters are similar to that of neutral ones, e.g. half-sandwich-type structures emerge at $n = 10$–13 and gradually transform to perfect double-ring tubular structures at $n = 16$, from which endohedral B cages are beginning to form. However, for a certain cluster size, there are more or less differences in the structures for different charge states. At $n = 10, 12, 13$, and 16, the structures at different charge states are almost identical except some divergence in the exact point group symmetries, which may due to the John–Teller effect, e.g. MnB$_{16}^-$ with double-ring tubular structure distorted from D_{8a} to C_{4v} symmetry due to the first-order Jahn–Teller effect, while neutral MnB$_{16}$ further distorted to C_{2v} symmetry due to the second-order Jahn–Teller effect [37]. Cluster at other sizes usually shows different structures in different charge states. At $n = 11$, the cationic species MnB$_{11}^+$ adopts similar structure as that of the neutral one, but the anionic species MnB$_{11}^-$ shows
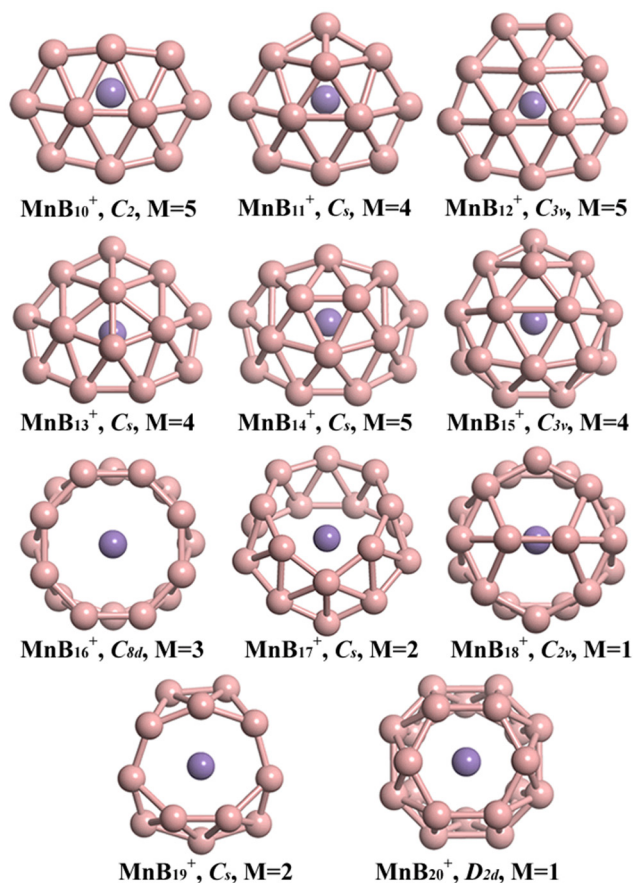
Figure 2. Lowest-energy structures of MnB_n^+ ($n = 10$–20) clusters from the structure searches. For each structure, the point group symmetry and spin multiplicity (M) are indicated.
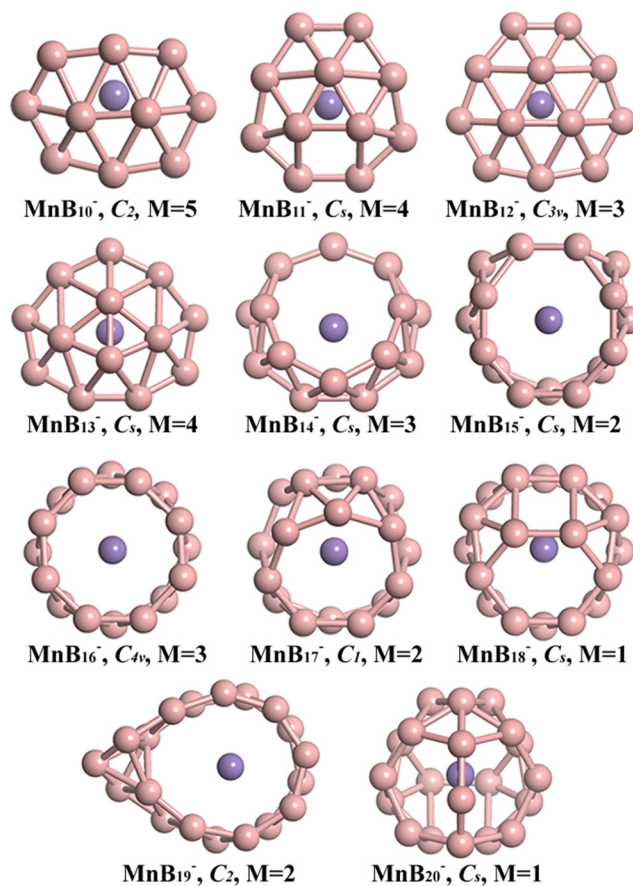

Figure 3. Lowest-energy structures of MnB_n^- ($n = 10$–20) clusters from the structure searches. For each structure, the point group symmetry and spin multiplicity (M) are indicated.

a different quasi-planar B_{11} moiety that contains a B quadrangle. At $n = 14$, the anionic species possesses similar structures as that of the neutral one with the B_{14} moiety contains an 8-membered ring, but the cationic one exhibits a bowl-like B_{14} moiety completely formed by B triangles. At $n = 15$, the bowl-like B_{15} moiety is completely formed by B triangles for the cationic species, while it is an incomplete double-ring tube for the anionic species. At $n = 17$, the cationic species possesses similar tubular B_{17} moiety as that of the neutral one, but the anionic species possesses a different tubular B_{17} moiety which can be seen as double-ring B_{16} tube with a capped B atom. At $n = 18$, structural differences for species at different charge states arise from the specific arrangements of the two capped B atoms. At $n = 19$, irregular cage-like B_{19} moieties emerge for neutral and cationic species, while tubular B structure persists for the anionic species. At $n = 20$, B cages are formed for both neural and charged species, and all of them are formed by B triangles and 6-membered rings. While the B_{20} cage for the anionic species is irregular, the ones for neutral and cationic species are more symmetric with point group symmetries of C_{3v} and D_{2d}, respectively.

It is noteworthy that several endohedral B cages can be formed when Mn atom is doped to larger B_n cluster, e.g. $MnB_{19}^{0/+}$ and $MnB_{20}^{0/+/-}$. Among them, MnB_{20}^+ shows a structure with relative high point group symmetry of D_{2d}, implying

its highly degenerated electronic states and potentially high chemical stability. For pure B clusters, most cage-like structures are formed at cluster size around 40 [27–30], and the smallest B cage is recently observed at B_{28} [15]. Previous theoretical studies have shown that transition demarcation to cage-like structures can be further reduced to $n = 18$ with the help of transition metal encapsulation [44, 45]. Especially when both electronic and geometric fit are satisfied, high symmetric endohedral B cages will emerge with relative high stabilities. For example, symmetric B_{24} cage with high stability can be produced through Mo or W doping, since interactions between Mo/W and B_{24} cage leads to the formation of an 18-electron closed-shell configuration (electronic fit) whilst the size of Mo/W just fit the void of the B_{24} cage (geometric fit) [45]. Below we will show that MnB_{20}^+ cluster is another such example.

3.2. Relative stabilities and HOMO-LUMO gaps

Frequency calculations confirm the dynamical stability by showing no imaginary frequency for all the global minimum structures and low-lying isomers shown in figures S1–S3. The corresponding lowest frequencies are listed in Table SI–SIII in the supplementary data. To assess the relative stabilities of the MnB_n^Q ($n = 10$–20 and $Q = 0, \pm1$) clusters, the averaged
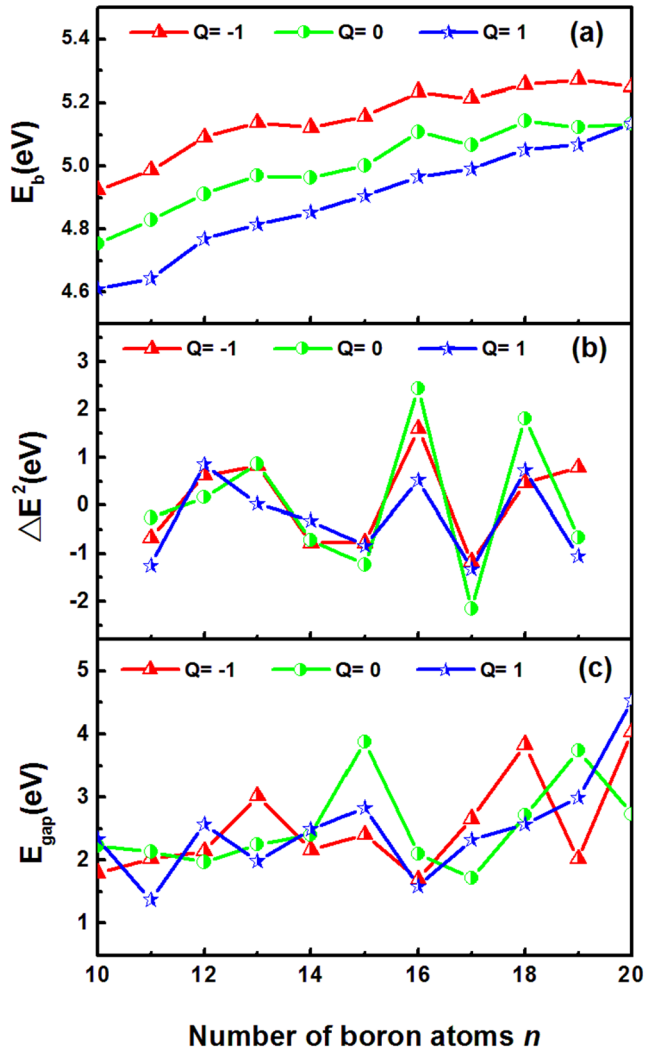
Figure 4. Size dependence of the averaged atomic binding energies $E_b(n)$, the second-order difference of energies $\Delta^2 E(n)$, and the HOMO-LOMO gaps E_{gap} for the lowest-energy structures of neutral and charged MnB_n^Q ($n = 10$–20, $Q = 0, \pm 1$) clusters.

atomic binding energies (E_b), second-order difference of energies ($\Delta^2 E$) and HOMO-LUMO gaps are calculated and shown in figure 4 as a function of the number of B atoms (n). The relative stabilities of clusters can be qualitatively estimated from E_b, which defined as

$$
\begin{aligned}
& E_b(MnB_n^{-/0/+}) \\
& = \left[\begin{array}{c} nE(B) + E(Mn)^{0/+} - E(MnB_n^{0/+}) \\ \text{or} \\ (n-1)E(B) + E(B^-) + E(Mn) - E(MnB_n^-) \end{array} \right] /(n+1)
\end{aligned}
\tag{1}
$$

where $E(B^{0/-})$ and $E(Mn^{0/+})$ are the total energies of the corresponding neutral and charged B and Mn atoms, and $E(MnB_n^{-/0+})$ are the total energies of the corresponding clusters. The larger E_b value indicates the higher thermodynamic stability of a cluster, because more energy (per atom) has been released during the formation process of the cluster. From figure 4(a), it is seen that the E_b values of anionic MnB_n^- clusters are the highest among those of $MnB_n^{-/0/+}$ clusters,

while cationic MnB_n^+ clusters possess the lowest E_b values. The E_b values for both neutral and charged clusters have an increasing tendency and show slight oscillations with increasing cluster size. For neutral MnB_n, three peak values of E_b occur at $n = 13$, 16 and 18, while anionic MnB_n^- have three peak values at $n = 13$, 16 and 19, indicating that the MnB_{13}, MnB_{16}, MnB_{18}, MnB_{13}^-, MnB_{16}^- and MnB_{19}^- clusters are relatively more stable than their neighbors. For cationic MnB_n^+, four peak values are observed at $n = 12$, 16, 18 and 20, indicating that MnB_{12}^+, MnB_{16}^+, MnB_{18}^+ and MnB_{20}^+ are more stable than their neighbors. The relative thermodynamic stabilities of neutral and charged $MnB_n^{-/0/+}$ clusters can also be obtained from the $\Delta^2 E$, which is defined as

$$
\begin{aligned}
\Delta^2 E(MnB_n^{-/0/+}) & = E(MnB_{n-1}^{-/0/+}) \\
& + E(MnB_{n+1}^{-/0/+}) - 2E(MnB_n^{-/0/+})
\end{aligned}
\tag{2}
$$

where $E(MnB_n^{-/0+})$ are the total energies of the corresponding clusters. As seen from figure 4(b), the $\Delta^2 E$ values as a function of cluster size give clear indications of the relative thermodynamic stabilities of a cluster compared with its neighbors. The results are exactly consistent with those obtain from E_b values. However, the relative stabilities of $MnB_{20}^{-/0/+}$ cannot be obtained from $\Delta^2 E$, since we have not considered $MnB_{21}^{-/0/+}$ in the current work.

HOMO-LUMO gap is another quantity that frequently used to characterize the electronic stabilities of clusters. It to some extent shows the ability of molecules or clusters to react to each other in chemical reactions. A larger value of HOMO-LUMO gap usually indicates a higher chemical stability. Our previous work has shown that using HOMO-LUMO gap as indicator for the chemical stability of clusters generally gives consistent result as that using chemical hardness [45]. The calculated HOMO-LUMO gaps for the lowest-energy $MnB_n^{-/0+}$ ($n = 10$–20) clusters as a function of the number of B atoms is presented in figure 4(c). Relative large HOMO-LUMO gaps were observed at $n = 15$, 19 for the neutral clusters, $n = 18$, 20 for the anions, and $n = 20$ for the cations, indicating relative high chemical stabilities of $MnB_n^{-/0+}$ clusters at these sizes and charge states. All of them possess even number of electrons with singlet spin states. Among them, MnB_{20}^+ cluster shows the highest HOMO-LUMO gap of 4.53 eV.

Previous studies have shown that both electronic and geometric factors play important roles in rational design of transition-metal doped B clusters [18, 52]. The formation of intriguing geometries needs not only the geometric fit between the size of the transition-metal atom and the B structures, but also the satisfaction of some specific electronic design principles (e.g. doubly aromaticity for transition-metal-centered borometallic molecular wheels [18, 52]). It is seen from current results that $MnB_{16}^{-/0/+}$ clusters with double-ring tubular B structures are always thermodynamically more stable than its neighbors regardless of the charge states, though they show relative small HOMO-LUMO gaps. This indicates geometric fit is satisfied, which significantly increases the robustness of the tubular B structures in Mn doped B_{16} clusters. Strikingly, an endohedral B cage with high symmetry of D_{2d} have been
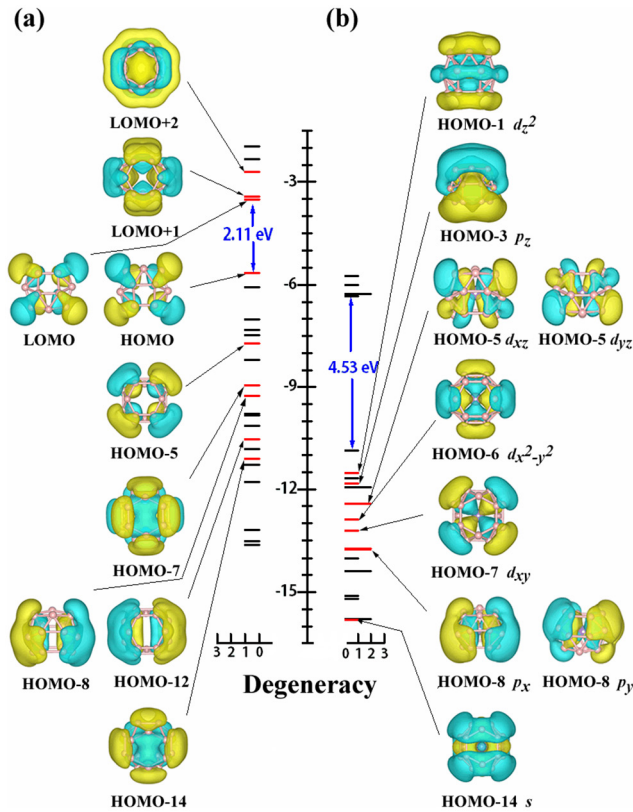
Figure 5. Eigenvalue spectra and electronic state degeneracy of (a) bare D_{2d}-B_{20} cage and (b) endohedral D_{2d}-MnB_{20}^+ cage. For each case, the HOMO-LUMO gap is indicated (in blue). The π-orbitals (red lines) for (a) and the orbitals involving 18-electron closed-shell configuration (see text) in (b) are shown. The corresponding isosurfaces of the molecular orbitals are given with isovalues of ± 0.02 au.

reveal as the global minimum structure for the MnB_{20}^+ cluster, which shows a superior thermodynamic stability and the largest HOMO-LUMO gaps among all $MnB_n^{-/0/+}$ clusters considered. This implies both electronic and geometric fits might be satisfied in this endohedral D_{2d}-MnB_{20}^+ cage.

3.3. Origin of the stability of the symmetric endohedral MnB_{20}^+ cage

The geometric factor responsible for the stability of the endohedral D_{2d}-MnB_{20}^+ cage is straightforward. Earlier theoretical studies by some of us have found that Mo or W atom doping will stabilized a symmetric B_{24} cage, but Cr atom with same number of valence electrons cannot [45]. This is due to the fact that Cr atom with smaller atomic radius (1.39 Å) compared with Mo (1.54 Å) or W (1.62 Å) is not optimal to fit the cavity of the B_{24} cage and leads to geometry frustration becoming energetically favorable in the structure. Mn with similar atomic radius (1.39 Å) as that of Cr is thus reasonably expected to be suitable for smaller B cages.

To reveal the electronic origin of the stability of the endohedral D_{2d}-MnB_{20}^+ cage, the chemical bonding of bare D_{2d}-B_{20} cage and endohedral D_{2d}-MnB_{20}^+ cage were analyzed based on canonical molecular orbitals (CMOs). According to

crystal field theory, interaction between the transition metal (Mn) and ligand (B_{20} cage) arises from the attraction between the positively charged metal cation and non-bonding electrons (electrons that transfer from Mn to B_{20} cage as well as π-electrons of the bare B_{20} cage) of the negatively charged ligand. It was found that the bare D_{2d}-B_{20} cage has 6 occupied π-CMOs (HOMO, HOMO-5, -7, -8, -12 and -14) and thus 12 π-electrons. Mn has an electron configurations of $[Ar]4s^24d^5$ with seven valence electrons. The $+1$ charge state of MnB_{20}^+ leads to the reminiscent of the well-known transition metal complexes, such as ferrocence $Fe(C_5H_5)_2$ and chromium hexacarbonyl $Cr(CO)_6$. In each complex, the ligand contributes 12 electrons and the central transition metal contributes six electrons, forming an 18-electron closed-shell configuration. Thus the stability of the endohedral D_{2d}-MnB_{20}^+ cage is expected to be attributed to the formation of 18-electron configuration. Indeed, the bare D_{2h}-B_{20} cage has three unoccupied π-CMOs (LUMO, LUMO + 1 and LUMO + 2 (figure 5)), which make it a π-acceptor ligand that interact with the valence electrons of Mn atom. From the shapes of CMOs in D_{2d}-MnB_{20}^+, nine CMOs (18 electrons) that are involved in the 'spd-π interaction' [53] have been identified (figure 5). HOMO-14 can be view as a super s-π orbital, originated from the $4s$ orbital of Mn and π orbital of B_{20} cage. HOMO-5 ($3d_{xz}$-π and $3d_{yz}$-π orbitals), HOMO-8 ($6p_y$-π and $6p_x$-π orbitals) are all double-degenerate orbitals. HOMO-7, HOMO-6, HOMO-3 and HOMO-1 can be view as $3d_{xy}$-π, $3d_{x^2-y^2}$-π, $4p_z$-π and $5d_{z^2}$-π orbitals, respectively. Projected density of states and results of orbital composition analysis for the D_{2d}-MnB_{20}^+ are given in figure S4 and table SIV in the supplementary data, respectively, which manifest that the Mn-B bondings mainly come from the above identified 9 CMOs. Thus the stability of D_{2d}-MnB_{20}^+ is attributed to the formation of 18-electron closed-shell configuration due to the mutual interaction between the π-electrons of the B cage and valence electrons of Mn. This has significantly increased the HOMO-LUMO gap from 2.11 eV of the bare D_{2d}-B_{20} cage to 4.53 eV of endohedral D_{2d}-MnB_{20}^+ cage, resulting in substantial energy gain to increasing structural stability of the endohedral D_{2d}-MnB_{20}^+ cage.

4. Conclusions

In summary, we have performed an unbiased first-principle structure search study for MnB_n^Q clusters with $n = 10$–20 and $Q = 0, \pm 1$. Putative global minimum structures have been proposed. It is found that Mn doping has fundamentally modified the grow behaviors of B clusters, leading to two structural transitions from planar to tubular and then to cage-like B structures in both neutral and charged species. While half-sandwich-type structures favor for small $MnB_n^{-/0/+}$ ($n \leqslant 13$) clusters, Mn-centered double-ring tubular structures emerge at $MnB_{16}^{-/0/+}$ clusters with superior thermodynamic stabilities compared with their neighbors. Larger $MnB_n^{-/0/+}$ ($n \geqslant 19$) clusters adopt endohedral cage-like structures, among which MnB_{20}^+ cluster possesses a highly symmetric structure with

superior thermodynamic stability and the largest HOMO-LUMO gap among all $MnB_n^{-/0/+}$ $(10 \leqslant n \leqslant 20)$ clusters considered. The stability of the endohedral D_{2d}-MnB_{20}^+ cage is attributed to the geometric fit between the size of the Mn atom and the cavity of the B cage as well as the formation of the 18-electron closed-shell configuration. The current results imply that with reasonable choices of transition metal atom and appropriate number of boron atoms, other sized boron cages are also likely to be stabilized, and thus leading to a rich variety of endohedral boron cages with high stability and fascinating properties. The current results will inevitably stimulate further theoretical and experimental efforts on the discovery of more intriguing B-based clusters.

Acknowledgments

Supplementary data

Supplementary data associated with this article can be found, in the online version.

References

[1] Albert B and Hillebrecht H 2009 *Angew. Chem. Int. Ed.* **48** 8640–68
[2] Mannix A J *et al* 2015 *Science* **350** 1513–6
[3] Bezugly V, Kunstmann J, Grundkötter-Stock B, Frauenheim T, Niehaus T and Cuniberti G 2011 *ACS Nano* **5** 4997–5005
[4] Kunstmann J, Bezugly V, Rabbel H, Rümmeli M H and Cuniberti G 2014 *Adv. Funct. Mater.* **24** 4127–34
[5] Ciuparu D, Klie R F, Zhu Y and Pfefferle L 2004 *J. Phys. Chem.* B **108** 3967–9
[6] Liu F, Shen C, Su Z, Ding X, Deng S, Chen J, Xu N and Gao H 2010 *J. Mater. Chem.* **20** 2197
[7] Huang W, Sergeeva A P, Zhai H-J, Averkiev B B, Wang L-S and Boldyrev A I 2010 *Nat. Chem.* **2** 202–6
[8] Piazza Z A, Li W-L, Romanescu C, Sergeeva A P, Wang L-S and Boldyrev A I 2012 *J. Chem. Phys.* **136** 104310
[9] Piazza Z A, Popov I A, Li W-L, Pal R, Cheng Zeng X, Boldyrev A I and Wang L-S 2014 *J. Chem. Phys.* **141** 34303
[10] Popov I A, Piazza Z A, Li W-L, Wang L-S and Boldyrev A I 2013 *J. Chem. Phys.* **139** 144307
[11] Romanescu C, Harding D J, Fielicke A and Wang L-S 2012 *J. Chem. Phys.* **137** 14317
[12] Sergeeva A P, Averkiev B B, Zhai H-J, Boldyrev A I and Wang L-S 2011 *J. Chem. Phys.* **134** 224304
[13] Sergeeva A P, Piazza Z A, Romanescu C, Li W-L, Boldyrev A I and Wang L-S 2012 *J. Am. Chem. Soc.* **134** 18065–73
[14] Sergeeva A P, Zubarev D Y, Zhai H, Boldyrev A I and Wang L 2008 *J. Am. Chem. Soc.* **130** 7244–6
[15] Wang Y-J *et al* 2016 *J. Chem. Phys.* **144** 64307
[16] Zhai H-J, Alexandrova A N, Birch K A, Boldyrev A I and Wang L-S 2003 *Angew. Chem. Int. Ed.* **42** 6004–8
[17] Zhai H-J, Kiran B, Li J and Wang L-S 2003 *Nat. Mater.* **2** 827–33
[18] Sergeeva A P, Popov I A, Piazza Z A, Li W-L, Romanescu C, Wang L-S and Boldyrev A I 2014 *Acc. Chem. Res.* **47** 1349–58
[19] Zubarev D Y and Boldyrev A I 2007 *J. Comput. Chem.* **28** 251–68
[20] Ogitsu T, Schwegler E and Galli G 2013 *Chem. Rev.* **113** 3425–49
[21] Oger E, Crawford N R M, Kelting R, Weis P, Kappes M M and Ahlrichs R 2007 *Angew. Chem. Int. Ed.* **46** 8503–6
[22] Kiran B, Bulusu S, Zhai H-J, Yoo S, Zeng X C and Wang L-S 2005 *Proc. Natl Acad. Sci. USA* **102** 961–4
[23] Li W-L, Chen Q, Tian W-J, Bai H, Zhao Y-F, Hu H-S, Li J, Zhai H-J, Li S-D and Wang L-S 2014 *J. Am. Chem. Soc.* **136** 12257–60
[24] Li W-L, Pal R, Piazza Z A, Zeng X C and Wang L-S 2015 *J. Chem. Phys.* **142** 204305
[25] Li W-L, Zhao Y-F, Hu H-S, Li J and Wang L-S 2014 *Angew. Chem.* **126** 5646–51
[26] Piazza Z A, Hu H-S, Li W-L, Zhao Y-F, Li J and Wang L-S 2014 *Nat. Commun.* **5** 1–6
[27] Lv J, Wang Y, Zhu L and Ma Y 2014 *Nanoscale* **6** 11692–6
[28] Zhai H-J *et al* 2014 *Nat. Chem.* **6** 727–31
[29] Chen Q *et al* 2015 *ACS Nano* **9** 754–60
[30] Chen Q *et al* 2015 *Angew. Chem. Int. Ed.* **54** 8160–4
[31] Alexandrova A N, Boldyrev A I, Zhai H-J and Wang L-S 2006 *Coord. Chem. Rev.* **250** 2811–66
[32] Popov I A, Li W, Piazza Z A, Boldyrev A I and Wang L 2014 *J. Phys. Chem.* A **118** 8098–105
[33] Romanescu C, Galeev T R, Sergeeva A P, Li W L, Wang L S and Boldyrev A I 2012 *J. Organomet. Chem.* **721–2** 148–54
[34] Romanescu C, Galeev T R, Li W-L, Boldyrev A I and Wang L-S 2011 *Angew. Chem. Int. Ed.* **50** 9334–7
[35] Li W, Romanescu C, Galeev T R, Piazza Z A, Boldyrev A I and Wang L 2012 *J. Am. Chem. Soc.* **134** 165–8
[36] Galeev T R, Romanescu C, Li W-L, Wang L-S and Boldyrev A I 2012 *Angew. Chem. Int. Ed.* **51** 2101–5
[37] Jian T, Li W-L, Popov I A, Lopez G V, Chen X, Boldyrev A I, Li J and Wang L-S 2016 *J. Chem. Phys.* **144** 154310
[38] Popov I a, Jian T, Lopez G V, Boldyrev A I and Wang L-S 2015 *Nat. Commun.* **6** 8654
[39] Bai H, Chen Q, Zhai H-J and Li S-D 2015 *Angew. Chem. Int. Ed.* **54** 941–5
[40] Chen Q, Li H-R, Miao C-Q, Wang Y-J, Lu H-G, Mu Y-W, Ren G-M, Zhai H-J and Li S-D 2016 *Phys. Chem. Chem. Phys.* **18** 11610–5
[41] Fa W, Chen S, Pande S and Zeng X C 2015 *J. Phys. Chem.* A **119** 11208–14
[42] Jin P, Hou Q, Tang C and Chen Z 2015 *Theor. Chem. Acc.* **134** 13
[43] Lu Q L, Luo Q Q, Li Y D and Huang S G 2015 *Phys. Chem. Chem. Phys.* **17** 20897–902
[44] Tam N M, Pham H T, Duong L V, Pham-Ho M P and Nguyen M T 2015 *Phys. Chem. Chem. Phys.* **17** 3000–3
[45] Lv J, Wang Y, Zhang L, Lin H, Zhao J and Ma Y 2015 *Nanoscale* **7** 10482–9
[46] Wang Y, Lv J, Zhu L and Ma Y 2010 *Phys. Rev.* B **82** 94116
[47] Wang Y, Lv J, Zhu L and Ma Y 2012 *Comput. Phys. Commun.* **183** 2063–70
[48] Lv J, Wang Y, Zhu L and Ma Y 2012 *J. Chem. Phys.* **137** 84104
[49] Frisch M J *et al* 2009 Gaussian 09, revision C.01, Gaussian, Inc., Wallingford, CT
[50] Adamo C and Barone V 1999 *J. Chem. Phys.* **110** 6158
[51] Li F, Jin P, Jiang D, Wang L, Zhang S B, Zhao J and Chen Z 2012 *J. Chem. Phys.* **136** 74302
[52] Romanescu C, Galeev T R, Li W-L, Boldyrev A I and Wang L-S 2013 *J. Chem. Phys.* **138** 134315
[53] Yan Y and Cheng L 2013 *J. Chem. Phys.* **138** 024301